Desalination and Water Treatment
www.deswater.com

doi: 10.5004/dwt.2021.26620

211 (2021) 241–249
January

$Co(OH)_2$/red phosphorus photocatalyst with spatially separated co-catalyst for efficient oxidation and reduction of pollutants

Yuhua Ma[#], Yun Wang[#], Hong Du, Lu Xiao*, Abudusaimi Abulikemu

College of Chemistry and Chemical Engineering, Xinjiang Normal University, Urumqi, 830054, China, Tel. +86-991-4332091; emails: ange_lu0529@163.com (L. Xiao), 15199141253@163.com (Y. Ma), 26083289@qq.com (Y. Wang), 175790509@qq.com (H. Du), 1319890694@qq.com (A. Abulikemu)

Received 1 May 2020; Accepted 15 September 2020

ABSTRACT

$Co(OH)_2$ is an effective co-catalyst that can augment the photocatalytic activity of the hydrothermal-treated red phosphorus (HRP) semiconductor. The results of composition proportion optimization showed that $Co(OH)_2$/HRP photocatalyst displayed supreme photocatalytic activity when the mass fraction of $Co(OH)_2$ was 0.25%, the photocatalytic rate constants for rhodamine B and Cr(VI) were 4.0×10^{-2} and 7.0×10^{-2} min^{-1}, respectively, which were 2 and 2.4 times higher than that of pure HRP. Therefore, $Co(OH)_2$ can act as an efficient co-catalyst that can significantly enhance the crystallinity, specific surface area, photoresponse range and photocurrent responses, and photogenerated electron and hole separation of HRP.

Keywords: Red phosphorus; $Co(OH)_2$; Nanocomposites; Oxidation; Reduction

1. Introduction

Among elemental photocatalysts, red phosphorus (RP) is the most promising [1,2]. However, it is amorphic and has a large size and low dispersion, which cause serious recombination problem of its photogenerated carriers and result in poor photocatalytic activity [3,4]. Several methods have been introduced to improve the photocatalytic ability of RP, including morphological modulation [5,6], heterojunction structure [4,7,8], Schottky junction [9], immobilization [3]. Among these approaches, the adoption of co-catalyst for surface modification is the most effective method to inhibit the rapid recombination of photogenerated electron–hole pairs and provide effective active sites. In addition, the modification of the co-catalyst is usually conducted under mild experimental conditions. Thus, the crystal structure of the main photocatalyst can be well-preserved, and the photocatalytic activity can be improved greatly by loading a small amount of co-catalyst [10]. In summary, the modification of the co-catalyst is an important and effective method to improve the photocatalytic activity of photocatalysts.

Noble metals (e.g., Pt, Au and Pd) have been widely used as surface modifiers to improve the photocatalytic performance [11–13]. However, their rarity and high cost limit their widespread application. Low-cost and earth-abundant co-catalysts should be explored for the development of photocatalysis. $Co(OH)_2$ is low-cost and its hydroxide can efficiently enhance electron transfer, charge separation and charge carrier lifetime [10]. Thus, it is an efficient co-catalyst that can significantly enhance the photocatalytic activity of semiconductors [11,14]. The $Co(OH)_2$ nanoparticles were first proposed as co-catalyst to modify the surface of Fe_2O_3 nanoparticles, and found that this strategy can effectively improve the hydrogen production of the catalyst [15]. The $Co(OH)_2$ loaded on CdS nanowires can effectively accelerate the charge separation and transfer in photocatalytic reaction, and the hydrogen production of the catalyst with

* Corresponding author.

[#] These authors contributed equally.

the best loading amount of $Co(OH)_2$ was 14.43 mmol h^{-1} g^{-1}, 206 times that of CdS [14]. The $Co(OH)_2$ implanted was into g-C_3N_4 uniformly by in-situ chemical deposition method. This experiment confirmed that the strong interaction between $Co(OH)_2$ and g-C_3N_4 can advance the transfer rate of photogenerated electron to reduce the charge carries recombination, and therefore can increase the hydrogen production rate of the catalyst [11]. The above reports indicate that $Co(OH)_2$ is a co-catalyst that can effectively improve the photocatalytic activity of the catalysts.

This study aims to develop a high-efficiency photocatalyst, which is made of abundant $Co(OH)_2$ and hydrothermal-treated RP. It is used not only to stimulate the photo-oxidation capacity of hydrothermal-treated red phosphorus (HRP) but also to improve its photo-reduction capacity for efficiently treating organic pollutant and heavy metal in wastewater. This study provides a new pathway for developing efficient photocatalytic materials for comprehensive wastewater treatment.

2. Experimental setup

2.1. Preparation of $Co(OH)_2$/HRP

Pretreatment of red phosphorus: 0.6 g commercial red phosphorus was added into hydrothermal reactor, and hydrothermally treated at 200°C for 16 h, the sample was subsequently washed and dried at 80°C for 5 h to obtain the HRP powder.

Synthesis of $Co(OH)_2$: 0.98 g $Co(NO)_3$, 0.864 g NaOH and 0.232 g EDTA were heated in 50 mL deionized water by water bath at 55°C, and 0.076 g glucose was added after 5 min. The mixed solution was heated in water bath and well dispersed at 60°C for 1 h. After washed and dried (80°C, 5 h), the $Co(OH)_2$ powder was accomplished.

$Co(OH)_2$ was mixed with HRP in different mass ratio (0.1%, 0.25%, 0.5%, 1%, 2%), then dispersed in 20 mL of distilled water, hydrothermally reacted at 150°C for 4 h, washed and dried to obtain the target products $Co(OH)_2$/HRP. The different ratios were labeled as 0.1%$Co(OH)_2$/HRP, 0.25%$Co(OH)_2$/HRP, 0.5%$Co(OH)_2$/HRP, 1%$Co(OH)_2$/HRP and 2%$Co(OH)_2$/HRP.

2.2. Characterization of $Co(OH)_2$/HRP photocatalyst

The crystal structure and phase composition of photocatalyst were determined by X-ray diffraction (XRD) (D8 Advance, Bruker, USA), which operating at 50 kV and 200 mA equipped with Cu-Kα radiation (λ = 1.54178 Å) at a scan rate of 6°/min; The particle diameter and electrical charge were measured using zeta potentiometer (ZS90, Malvern, Britain). The structure and dispersion of catalyst were analyzed by high magnification transmission electron microscopy (JEM-2010F, Hitachi, Japan); Specific surface area and pore distribution of sample were determined using Brunauer–Emmett–Teller (BET) (Micromeritics, ASAP 2400, USA). The absorption of UV-light was recorded using UV-vis Diffuse spectrophotometer (CARY300, Agilent, USA), which scanned in the wavelength range of 200–1,000 nm and used $BaSO_4$ (spectrum pure) as the reflectance standard; electrochemical properties were measured on a electrochemical workstation (CHI660E, Chenhua, China) using a standard three-electrode, the working electrode was installed using prepared catalyst, a Pt electrode as the counter electrode and an Ag/AgCl as the reference electrode, Na_2SO_4 (0.1 M) was used as the electrolyte solution.

2.3. Photocatalytic test of $Co(OH)_2$/HRP

5 mg $Co(OH)_2$/HRP was added into 20 mL RhB (10 mg/L) and 20 mL Cr(VI) (40 mg/L) solution respectively, magnetic stirring for 30 min in the dark to achieve adsorption–desorption equilibration and was stirred continuously during irradiation, 3 mL supernatant was filtered every 10 min. The residual pollutants concentration in the supernatant was determined at 356 nm (Cr(VI)) or 554 nm (RhB) with a UV-vis spectrometer. The degradation rate was calculated by the following Eq. (1):

$$\text{Degradation rate} = \frac{C_t}{C_0} \tag{1}$$

where C_0 is the concentration of original solution, where C_t is the concentration of residual contaminants at different irradiation time.

3. Results and discussion

3.1. Characterization of HRP and 0.25%$Co(OH)_2$/HRP

The composite photocatalysts were characterized by XRD and zeta potentiometer to analyze the crystal structure, particle size and electronic charge of $Co(OH)_2$/HRP, respectively. As shown in Fig. 1a, the XRD patterns of HRP and $Co(OH)_2$/HRP had the diffraction peaks at 15.0° and 33.0°, which were consistent with the characteristic diffraction phase of RP in previous reports [3]. Obviously, only RP could be observed in HRP and 0.25%$Co(OH)_2$/HRP composite photocatalysts, and no characteristic diffraction peak of $Co(OH)_2$ was observed. This result was due to the low content and weak crystallinity of $Co(OH)_2$ and its high dispersion on the surface of HRP. Further observation showed that the peak of the RP at 15° changed with the addition of $Co(OH)_2$, the peak intensity increased, and the peak shape became wider, which indicated that the crystallinity increased and the particle size was reduced after the combination. The average particle size further was measured (Fig. 1b), and were 376 and 292 nm for HRP and 0.25%$Co(OH)_2$/HRP, respectively. The results revealed that modifying the surface of HRP using $Co(OH)_2$ could inhibit the agglomeration and further growth. In addition, the TEM-EDS was carried out to investigate the chemical composition of the 0.25%$Co(OH)_2$/HRP composite, shown in Fig. S1. The EDS spectrum confirms the presence of P, Co and O peaks, which gives good agreement with the expected composite of $Co(OH)_2$ and HRP.

Fig. 2 shows the TEM results of HRP and 0.25%$Co(OH)_2$/HRP composite. In Fig. 2a, serious agglomeration is observed in pure HRP. Meanwhile, HRP was dispersed uniformly in 0.25%$Co(OH)_2$/HRP composite (Fig. 2b). The $Co(OH)_2$ particles were evenly distributed on the surface of HRP as well. These phenomena indicated that the $Co(OH)_2$ and

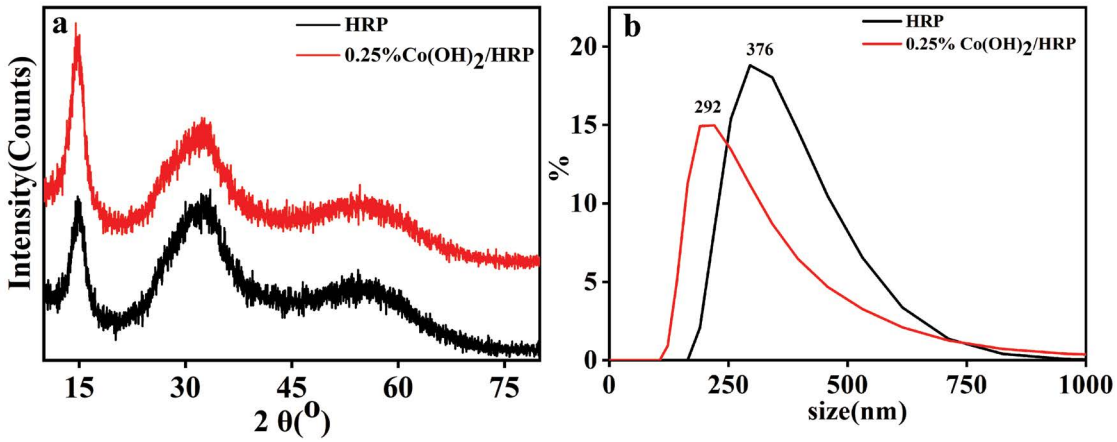

Fig. 1. XRD patterns (a) and particle size distribution (b) of HRP and 0.25%$Co(OH)_2$/HRP.

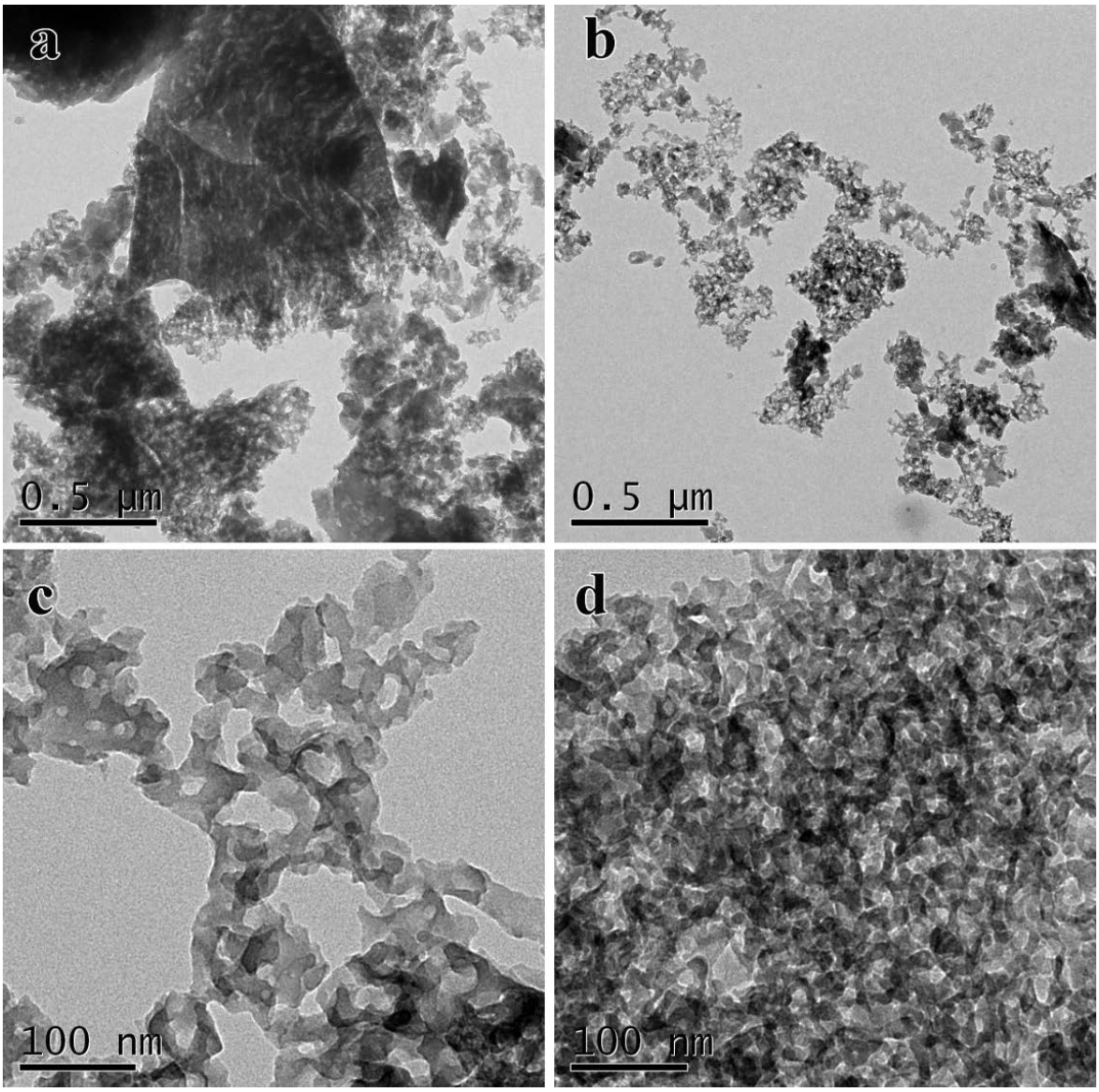

Fig. 2. TEM patterns of RP (a and c) and 0.25%$Co(OH)_2$/RP (b and d).

HRP had been compounded successfully, and the agglomeration problem of HRP had been solved accordingly. The TEM images of HRP and 0.25%$Co(OH)_2$/HRP composite photocatalyst were magnified. In Fig. 2c, neither the pore size nor the distribution of pure HRP is uniform. On the contrary, the pore diameter was richer and more even in 0.25%$Co(OH)_2$/HRP composite (Fig. 2d). The above-mentioned results confirmed that the $Co(OH)_2$ and HRP had been compounded successfully, which not only figured out the agglomeration problem but also minimized the particle size of HRP. This condition increased the contact area and probability with contaminated molecules in wastewater and improved the adsorptive and photocatalytic performance. Furthermore, the BET surface areas and pore-size distribution of samples were characterized, and the results are shown in Fig. S2. The N_2 adsorption–desorption isotherms of HRP and 0.25%$Co(OH)_2$/HRP composite were type IV (Brunauer–Deming–Deming–Teller classification), meaning the existence of mesopores. Moreover, the pore-size distributions are shown in the inset of Fig. S2, 0.25%$Co(OH)_2$/HRP composite exhibited unimodal distributions with the pore size centered at 22–50 nm, further determined the presence of mesopores. However, HRP displayed a very wide pore size distribution, which is mainly due to the aggregation among HRP particles (consistent with the TEM result). In addition, the surface area of HRP was 29 m^2/g, and the total pore volume was 0.21 cm^3/g. Meanwhile, the surface area of the 0.25%$Co(OH)_2$/HRP composite catalyst was 31 m^2/g, and the total pore volume was 0.22 cm^3/g, both increased after being compounded. The larger surface area of composite, the better the photodegradation performance of 0.25%$Co(OH)_2$/HRP in wastewater. Above characterization results revealed that HRP combined with $Co(OH)_2$ not only reduced its size and prevent agglomeration of nanoparticles but also increased its specific surface and pore volume. It was reasonable that the HRP is negatively charged (–35 mV), while $Co(OH)_2$ is positively charged (+48 mV). In a near neutral solution, negatively charged HRP and positively charged $Co(OH)_2$ are driven by mutual electrostatic interactions, which is the key to prevent HRP from excessive agglomeration.

3.2. Photocatalytic activity of HRP and 0.25%$Co(OH)_2$/HRP

Figs. 3a and c describe the photo-oxidation of RhB and photo-reduction of Cr(VI) by HRP and $Co(OH)_2$/HRP. The adsorption property and photocatalytic activity of $Co(OH)_2$/HRP enhanced first and then reduced whether for RhB or Cr(VI) with the increase of $Co(OH)_2$ mass fraction in HRP surface modification, the highest was obtained from the 0.25%$Co(OH)_2$/HRP composite. After dark adsorption for 30 min, the adsorption rates of RhB and Cr(VI) by 0.25%$Co(OH)_2$/RP composite were 54% and 40%, respectively, which were much higher than those of HRP (24% for RhB and 8% for Cr(VI)), especially for Cr(VI) (five times higher). Under visible-light irradiation for 90 min, the photo-oxidation rate of RhB and the photo-reduction rate

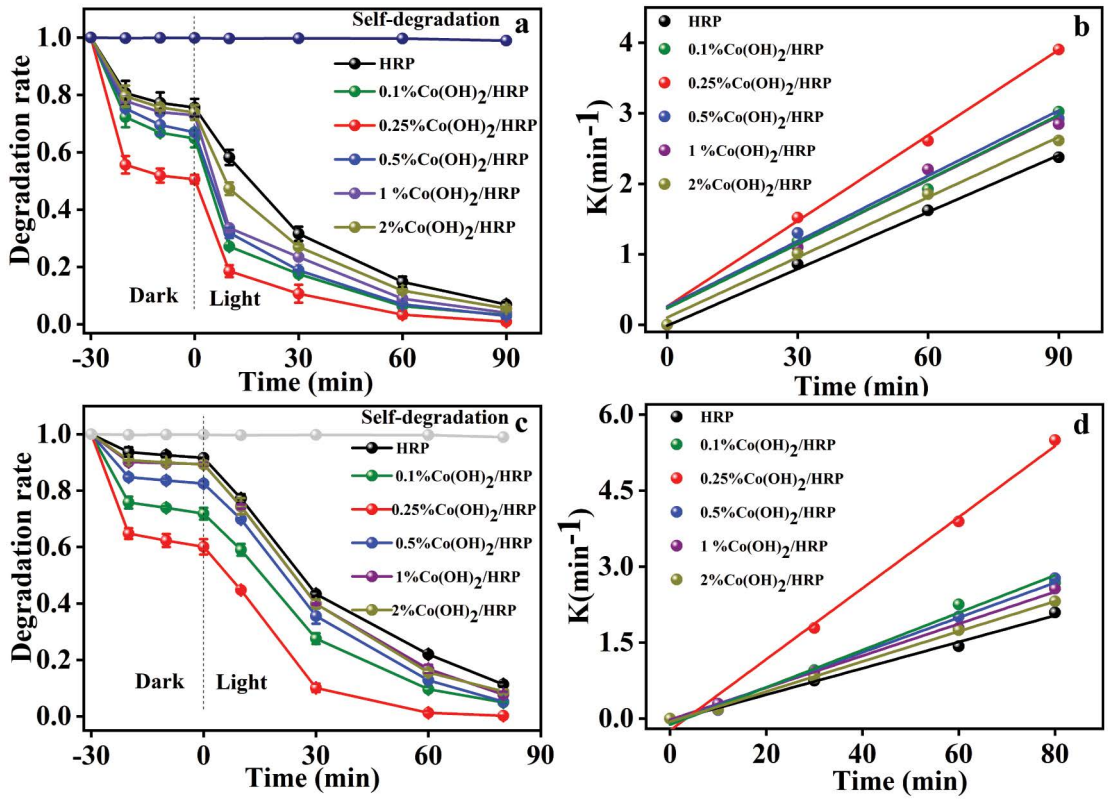

Fig. 3. Degradation of (a) RhB and (c) Cr(VI) by HRP, 0.1%$Co(OH)_2$/HRP, 0.25%$Co(OH)_2$/HRP, 0.5%$Co(OH)_2$/HRP, 1.0%$Co(OH)_2$/HRP, 2.0%$Co(OH)_2$/HRP; Reaction kinetics for (b) RhB photo-oxidation, and (d) Cr(VI) photo-reduction.

of Cr(VI) by 0.25%$Co(OH)_2$/RP composite (99% and 100%) exceed the values obtained by using HRP (92% and 89%), respectively.

Reaction kinetic studies showed that the photo-oxidation of RhB and photo-reduction of Cr(VI) by HRP and 0.25%$Co(OH)_2$/HRP followed the pseudo-first-order model:

$$\ln\left(\frac{C_0'}{C_t}\right) = -kt \quad (2)$$

where k is the photocatalytic rate constant (min^{-1}), C_0' is the concentration of contaminant that reach the adsorption–desorption equilibrium, C_t is the concentration of residual at certain interval.

As illustrated in Figs. 3b and d, the k values of 0.25% $Co(OH)_2$/HRP composite for RhB and Cr(VI) were 4.0×10^{-2} and 7.0×10^{-2} min^{-1}, respectively, which were 2 and 2.4 times those of HRP, respectively. In summary, modification of HRP with appropriate proportion of $Co(OH)_2$ could overcome the limitation and could thus improve the adsorptive and photocatalytic performance of HRP. The recoverability and stability of 0.25%$Co(OH)_2$/HRP composite photocatalyst was obtained and the results are shown in Fig. S3. The photocatalytic activity of the composite photocatalyst reached 92.7% after five cycles (Fig. S3a). Furthermore, it is hard to find difference from XRD images of the composite before and after five successive cycles of the reaction (Fig. S3b), which reflected that 0.25%$Co(OH)_2$/HRP composite photocatalyst can be used as an efficient and stable photocatalyst.

The photoabsorption and electron transport of 0.25% $Co(OH)_2$/HRP were investigated to detect the enhancement mechanism of photocatalytic activity. The photodegradation mechanism of pollutants by 0.25%$Co(OH)_2$/HRP was also verified by the active species trapping experiment.

The optical absorption properties of HRP and 0.25% $Co(OH)_2$/HRP were assessed by UV/Vis diffuse reflectance spectroscopy. As shown in Fig. 4a, the HRP shows a strong visible-light absorption range, which was based on appropriate band gap energy. Surprisingly, the 0.25%$Co(OH)_2$/HRP exhibited broader optical absorption and slightly weaker strength of light response in the visible region than HRP. This performance was due to the lower light harvesting efficiency of $Co(OH)_2$ [16]. The phenomenon was beneficial to expanding the visible-light response range and utilization of visible light [17].

Fig. 4b presents the photocurrent curve of HRP, 0.25% $Co(OH)_2$/HRP and 0.5%$Co(OH)_2$/HRP samples. The transient photocurrent responses of several switching cycles were recorded under intermittent irradiation. All of the samples showed a rapid and repeatable photocurrent response to each illumination. Then, the response dropped to close

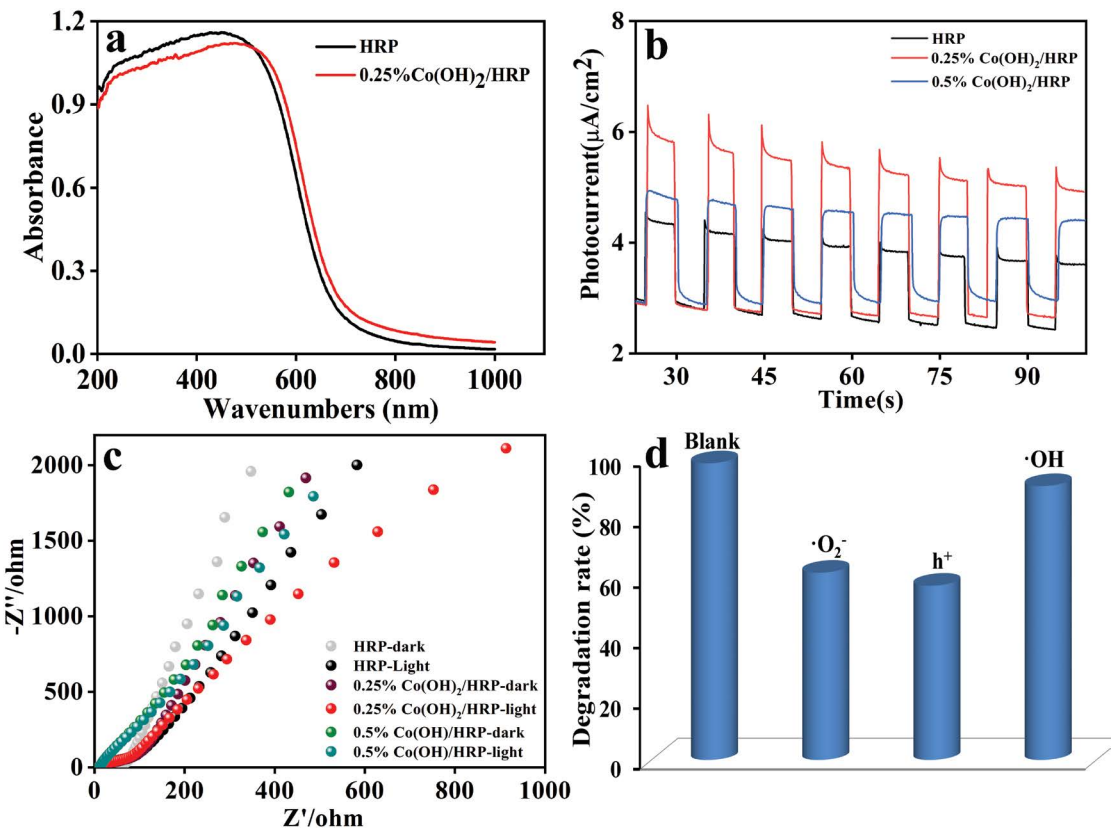

Fig. 4. (a) UV-vis diffuse reflectance spectra of HRP and 0.25%$Co(OH)_2$/HRP, (b) photoluminescence spectra of HRP, 0.25%$Co(OH)_2$/HRP and 0.5%$Co(OH)_2$/HRP, (c) electrochemical impedance spectroscopy of HRP, 0.25%$Co(OH)_2$/HRP and 0.5%$Co(OH)_2$/HRP in dark and light, and (d) the effect of different scavengers on the degradation of RhB in the presence of 0.25% $Co(OH)_2$/HRP.

zero promptly when the irradiation was switched off. The results showed that the photogenerated electrons could be transferred effectively through the sample to generate photocurrent under visible-light irradiation. As expected, the photocurrent of 0.25%$Co(OH)_2$/HRP was 2.4 times higher than that of HRP. Thus, 0.25%$Co(OH)_2$/HRP exhibited a high photocurrent response, which indicated a low electron–hole recombination. While, the photocurrent of 0.5%$Co(OH)_2$/HRP was lower than 0.25%$Co(OH)_2$/HRP, meaning the excess $Co(OH)_2$ loaded on HRP form a dense cover on the surface of HRP, which might shield the incident light irradiation and lead to reduced amount of photo-generated electrons.

In order to further prove the above conclusion that the photocarriers of the 0.25%$Co(OH)_2$/HRP photocatalyst possessed better separation efficiency between photogenerated electrons and holes, the electrochemical impedance spectroscopy (EIS) of pure HRP, 0.25%$Co(OH)_2$/HRP and 0.5%$Co(OH)_2$/HRP was carried out under visible light and dark conditions [18]. As shown in Fig. 4c, the arc radius of impedance curve by 0.25%$Co(OH)_2$/HRP was the smallest whether under light or dark conditions, suggesting the modification of HRP by modest $Co(OH)_2$ co-catalyst could accelerate the interfacial charge transfer, inhibited charge recombination and improve the photocatalytic ability of HRP. However, the impedance radius of 0.5%$Co(OH)_2$/HRP increased (i.e., the enlarged charge transfer resistance) due to the excessive addition of $Co(OH)_2$, which might act as new recombination center for photogenerated electrons and holes, hindering the migration of photogenerated electrons from the interior of the composite to the surface.

The abovementioned I-T and EIS characterizations had been verified that the HRP was modified by $Co(OH)_2$ could enhance the separation and transfer of photogenerated electrons and holes [19]. The conclusion was further confirmed by the Mott–Schottky characterization, and result is shown in Fig. S4. It could be observed from the figure that the Mott–Schottky plots of all samples exhibited a positive slope, which means that all samples are *n*-type semiconductors. The carrier concentrations were calculated using the slope of the linear region of the Mott–Schottky equation.

$$\frac{1}{C^2} = \left(\frac{2}{\varepsilon\varepsilon_0 A^2 e N_D}\right)\left(V - V_{\text{fb}} - \frac{\kappa_B T}{e}\right) \tag{3}$$

where C is interfacial capacitance, ε is the relative dielectric constant, ε_0 is the dielectric constant of the vacuum, A is the interfacial area, e is the electronic charge, N_D is the carrier concentration, V is the applied potential, V_{fb} is the flat band potential, κ_B is Boltzmann's constant and T is the absolute temperature. Since the value of $\kappa_B T/e$ is small at room temperature, it is negligible. From Fig. S4, it might be deduced that 0.25%$Co(OH)_2$/HRP composite had a higher carrier concentration (N_D) than pure HRP (N_D is inversely proportional to the slope of the Mott–Schottky plot), which is very favorable for the photocatalytic reaction.

The mechanism of enhancing photocatalytic activity could be summarized as follows. Under light irradiation for $Co(OH)_2$/HRP, the electrons (e^-) in valence band of HRP were excited to the conduction band. The $Co(OH)_2$ act as co-catalysts and electron traps to migrate electrons from the CB of HRP to the $Co(OH)_2$ surface, thus preventing the recombination of photogenerated electrons and holes and increasing the concentration of carriers (validated by I-T, EIS and Mott–Schottky). The trapped photogenerated electrons on the surface of $Co(OH)_2$ was involved in photoreduction of Cr(VI), and partials were captured by oxygen molecules dissolved in water to produce superoxide radical ($^{\bullet}O_2^-$). Simultaneously, an equal number of holes (h^+) was left in VB of HRP, while E_{VB} of HRP was inadequate for oxidizing H_2O to $^{\bullet}OH$ (2.38 eV) [7]. As a result, the $^{\bullet}O_2^-$ and h^+ active species could photodegrade RhB into water and CO_2 directly or indirectly. In addition, further experiments tested the effects of photocatalytic oxidation by adding radical trapping experiments including ammonium oxalate (AO), benzoquinone (BQ) and tert-butanol (TBA) to the 0.25%$Co(OH)_2$/HRP photocatalytic oxidation RhB system. Fig. 4d shows a slight effect of the addition of TBA on the degradation of RhB, which indicated that $^{\bullet}OH$ was not the primary reactive substance in the photocatalytic oxidation process. With the addition of BQ and AO, the efficiency decreased significantly, which implied that h^+ and $^{\bullet}O_2^-$ played a critical role in the photocatalytic oxidation process.

4. Conclusions

$Co(OH)_2$ co-catalyst was decorated on the surface of HRP to obtain the $Co(OH)_2$/HRP composite catalyst for improving the stability and dispersion of HRP. The 0.25%$Co(OH)_2$/HRP composite revealed the strongest adsorption and catalytic activity, the degradation rates for RhB and Cr(VI) were 2 and 2.4 times those of HRP, respectively. The enhanced mechanism revealed that the modification of the $Co(OH)_2$ on the surface of HRP enhanced photoresponsiveness, electron cloud density, and separation of photogenerated e^- and h^+.

Acknowledgments

This work was financially supported by Natural Science Foundation of Xinjiang Uygur Autonomous Region of China (2019D01B36, 2019D01A69), National Natural Science Foundation of China (52063028, 51968072), Natural Science Youth Project in Universities and Colleges of the Autonomous Region (XJEDU2018Y030), Electrochemistry Technology and Application Engineering Research Center (Engineering Center) Bidding Project (XJNUGCZX122017B04), Xinjiang Normal University.

References

[1] S.A. Ansari, M.S. Ansari, M.H. Cho, Metal free earth abundant elemental red phosphorus: a new class of visible light photocatalyst and photoelectrode materials, Phys. Chem. Chem. Phys., 18 (2016) 3921–3928.

[2] S.A. Ansari, Z. Khan, M.O. Ansari, M.H. Cho, Earth-abundant stable elemental semiconductor red phosphorus-based hybrids for environmental remediation and energy storage applications, RSC Adv., 6 (2016) 44616–44629.

[3] Y. Ma, D. Tuniyazi, M. Ainiwa, E. Zhu, Confined amorphous red phosphorus in metal–organic framework as a superior photocatalyst, Mater. Lett., 262 (2020) 127023–127027.

[4] X. Bai, J. Wan, J. Jia, X. Hu, Y. He, C. He, E. Liu, J. Fan, Simultaneous photocatalytic removal of Cr(VI) and RhB over 2D MoS_2/red phosphorus heterostructure under visible light irradiation, Mater. Lett., 222 (2018) 187–191.

[5] Z. Ren, D. Li, Q. Xue, J. Li, Y. Sun, R. Zhang, Y. Zhai, Y. Liu, Facile fabrication nano-sized red phosphorus with enhanced photocatalytic activity by hydrothermal and ultrasonic method, Catal. Today, 340 (2020) 115–120.
[6] D. Li, J. Li, Q. Jin, Z. Ren, Y. Sun, R. Zhang, Y. Zhai, Y. Liu, Photocatalytic reduction of Cr(VI) on nano-sized red phosphorus under visible light irradiation, J. Colloid Interface Sci., 537 (2019) 256–261.
[7] B. Xue, D. Yanyan, H. Xiaoyun, H. Yudong, H. Chunliang, L. Enzhou, F. Jun, Synergy removal of Cr(VI) and organic pollutants over RP-MoS_2/rGO photocatalyst, Appl. Catal., B, 239 (2018) 204–213.
[8] E.Q. Zhu, Y.H. Ma, H. Du, K.Z. Qi, M. Ainiwa, Z. Su, Three-dimensional bismuth oxide/red phosphorus heterojunction composite with enhanced photoreduction activity, Appl. Surf. Sci., 528 (2020) 146932–146940.
[9] L. Qi, K. Dong, T. Zeng, J. Liu, J. Fan, X. Hu, W. Jia, E. Liu, Three-dimensional red phosphorus: a promising photocatalyst with excellent adsorption and reduction performance, Catal. Today, 314 (2018) 42–51.
[10] Z. Li, Y. Wu, G. Lu, Highly efficient hydrogen evolution over $Co(OH)_2$ nanoparticles modified g-C_3N_4 co-sensitized by Eosin Y and Rose Bengal under visible light irradiation, Appl. Catal., B, 188 (2016) 56–64.
[11] S.C. Sun, Y.C. Zhang, G.Q. Shen, Y.T. Wang, X.L. Liu, Z.W. Duan, L. Pan, X.W. Zhang, J.J. Zou, Photoinduced composite of Pt decorated $Ni(OH)_2$ as strongly synergetic cocatalyst to boost H_2O activation for photocatalytic overall water splitting, Appl. Catal., B, 243 (2019) 253–261.
[12] G. Zhang, H. Miao, X. Hu, J. Mu, X. Liu, T. Han, J. Fan, E. Liu, Y. Yin, J. Wan, A facile strategy to fabricate Au/TiO_2 nanotubes photoelectrode with excellent photoelectrocatalytic properties, Appl. Surf. Sci., 391 (2017) 345–352.
[13] C. Han, M. Yang, N. Zhang, Y. Xu, Enhancing the visible light photocatalytic performance of ternary CdS-(graphene-Pd) nanocomposites via a facile interfacial mediator and co-catalyst strategy, J. Mater. Chem. A, 2 (2014) 19156–19166.
[14] X. Zhou, J. Jin, X. Zhu, J. Huang, J. Yu, W.-Y. Wong, W.-K. Wong, New $Co(OH)_2$/CdS nanowires for efficient visible light photocatalytic hydrogen production, J. Mater. Chem. A, 4 (2016) 5282–5287.
[15] H. Wender, R.V. Gonçalves, C.S.B. Dias, M.J. Zapata, L.F. Zagonel, E.C. Mendonça, S.R. Teixeira, F. Garcia, Photocatalytic hydrogen production of $Co(OH)_2$ nanoparticle-coated α-Fe_2O_3 nanorings, Nanoscale, 5 (2013) 9310–9316.
[16] D.P. Sahoo, S. Nayak, K.H. Reddy, S. Martha, K. Parida, Fabrication of a $Co(OH)_2$/ZnCr LDH "*p-n*" heterojunction photocatalyst with enhanced separation of charge carriers for efficient visible-light-driven H_2 and O_2 evolution, Inorg. Chem., 57 (2018) 3840–3854.
[17] D.X. Yang, D. Qu, X. Miao, W.S. Jiang, L. An, Y.J. Wen, D.D. Wu, Z.C. Sun, TiO_2 sensitized by red-, green-, blue-emissive carbon dots for enhanced H_2 production, Rare Met., 38 (2019) 404–412.
[18] C.Q. Han, J. Li, Z.Y. Ma, H.Q. Xie, G.I.N. Waterhouse, L.Q. Ye, T.R. Zhang, Black phosphorus quantum dot/g-C_3N_4 composites for enhanced CO_2 photoreduction to CO, Sci. China Mater., 61 (2018) 1159–1166.
[19] Y.F. Zhao, Y.X. Zhao, G.I.N. Waterhouse, L.R. Zheng, X.Z. Cao, F. Teng, L.Z. Wu, C.H. Tung, D. O'Hare, T.R. Zhang, Layered-double-hydroxide nanosheets as efficient visible-light-driven photocatalysts for dinitrogen fixation, Adv. Mater., 29 (2017) 1703828–1703838.

Appendix A

dV/*d*log(*W*) pore volume vs. pore width	
dV/*d*log(*W*) pore volume	
Pore width (Å)	*dV*/*d*log(*W*) pore volume (cm^3/g)
14.8328933786574	0
15.9051505362602	0.0388693105938657
17.1561170781044	0.0253298585958001
18.5857930041902	0.00740120466735674
20.0154697824296	0
21.623856797064	0
23.4109523437864	0
25.1980478905089	0
27.3425622057143	0.00399570599711173
29.4870765209197	0.00050324846310604
31.8103010725204	0
34.312235860516	0
36.9928791805996	0
40.0309395648592	0
43.2477135941281	0
46.6431944511778	0.00249429173743851
50.3960957810177	0.00788348541966978
54.3277039386385	0.00792586476785319
58.7954428054445	0.00788030805501097
63.4418919086456	0.0114749843160442
68.4457580760227	0.0134193588686491
73.9857583611993	0.014841589023885
79.8831723019375	0.0203846156946366
86.3167135432468	0.035851098980717
93.1076752573463	0.0427661493082516
100.613477917026	0.0419390815267461
108.655407877277	0.0485937085930124
117.233465138099	0.0552089272347664
126.52637016173	0.0784136035493514
136.712809324264	0.0899173992223205
147.61408943238	0.11749549760597
159.408917313856	0.127013065967299
172.097306603151	0.157915395506647
185.85793685913	0.192767598169776
200.69083535071	0.202497175032078
216.595974808974	0.244127016164064
233.930796158398	0.290335131258671
252.51660620566	0.318533647921258
272.710791337406	0.338969862383146
294.513351553636	0.27767297345044
317.924286854352	0.300199895643979
343.301065432941	0.423363425800426
370.643605482663	0.417762650352999
400.30940246582	0.379392027882167
432.298401844586	0.253841087325444
466.789378619025	0.228466806669468
503.96094417572	0.276699888296279

544.170593976974	0.238158016875753
587.596993947198	0.156386176624859
634.418919086456	0.135841762192259
684.993701243569	0.131137798132242
739.678835880841	0.0628105286063324
798.65298892268	0.0426027683528535
862.452321755802	0.044109642470245
931.255445766787	0.0397366816440706
1005.59868595583	0.0314746317973726
1085.66054463386	0.0354090160033799
1172.3346786499	0.054024022334385
1265.79975392835	0.045869138595452
1366.77065231817	0.0508369035601124
1475.9622556683	0.0732191806676419
1593.55312082751	0.0542742826974535
1720.79434556927	0.0499637484753372
1858.04315266677	0.0614927644596984
2006.19341712032	0.042510326111923
2166.31713447638	0.0391470848387869
2339.12940473523	0.0367157223124183
2525.70222344331	0.0338401387538617
2727.28647022281	0.041622447710031
2944.77612914972	0.0287916860284725
3179.77919354371	0.0265450332449362
3433.36787710257	0.0326671791202115
3707.32971167564	0.0225916950222117
4003.0940246582	0.0274049982544522

Appendix B

$dV/d\log(W)$ pore volume	
Pore width (Å)	$dV/d\log(W)$ pore volume (cm³/g)
14.8328933786574	0
15.9051505362602	0.0232261554339254
17.1561170781044	0.0180058094606417
18.5857930041902	0.0104815898721339
20.0154697824296	0
21.623856797064	0
23.4109523437864	0
25.1980478905089	0.00521146916071603
27.3425622057143	0.0103288867092915
29.4870765209197	0.00724270541606636
31.8103010725204	0.00629415331681044
34.312235860516	0.00122758820402461
36.9928791805996	0
40.0309395648592	0.00114407421032596
43.2477135941281	0.00587358195884145
46.6431944511778	0.00953603634641176
50.3960957810177	0.0110822380788156
54.3277039386385	0.0123485926905178
58.7954428054445	0.0116089827026285
63.4418919086456	0.0122346703769619
68.4457580760227	0.0154434482738187
73.9857583611993	0.017409523718702
79.8831723019375	0.0217966078480985
86.3167135432468	0.035128957979746
93.1076752573463	0.0412882833661144
100.613477917026	0.0421243627725154
108.655407877277	0.0504065987014957
117.233465138099	0.0566408707536254
126.52637016173	0.0777125163741684
136.712809324264	0.0901888124564456
147.61408943238	0.121715947030503
159.408917313856	0.131004176730338
172.097306603151	0.160209531897265
185.85793685913	0.201662541746138
200.69083535071	0.239922486663978
216.595974808974	0.30176637850178
233.930796158398	0.328815761301922
252.51660620566	0.322014540060769
272.710791337406	0.323342890101283
294.513351553636	0.275608495286805
317.924286854352	0.311262062403796
343.301065432941	0.43059891782069
370.643605482663	0.433890197848836
400.30940246582	0.423495070233139
432.298401844586	0.299479967043798
466.789378619025	0.270267998074716
503.96094417572	0.318690303926509
544.170593976974	0.243210607745822
587.596993947198	0.138620798523099
634.418919086456	0.107903231764159
684.993701243569	0.114636156920307
739.678835880841	0.0696709967505847
798.65298892268	0.0579910052534892
862.452321755802	0.0664423368022695
931.255445766787	0.0572509615605352
1005.59868595583	0.0389540049579977
1085.66054463386	0.035772512140756
1172.3346786499	0.0439931979669448
1265.79975392835	0.0304284336938189
1366.77065231817	0.0279617681136607
1475.9622556683	0.0344153651830998
1593.55312082751	0.0238217619800209
1720.79434556927	0.0219071340291864
1858.04315266677	0.0269734317118562
2006.19341712032	0.0186528050863279
2166.31713447638	0.0171654105825717
2339.12940473523	0.0161107651108094
2525.70222344331	0.0148383294506673
2727.28647022281	0.0182578627226208
2944.77612914972	0.0126337952770663
3179.77919354371	0.0116396919035891
3433.36787710257	0.0143297712038927
3707.32971167564	0.00991313469072851
4003.0940246582	0.0120426347512346

Supplementary information

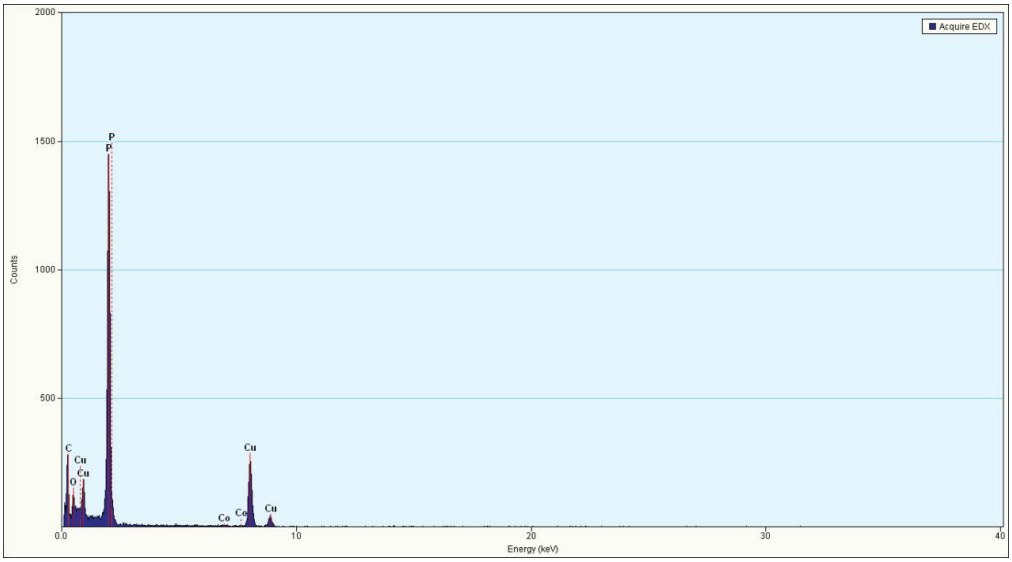

Fig. S1. EDS of 0.25%$Co(OH)_2$/HRP composite.

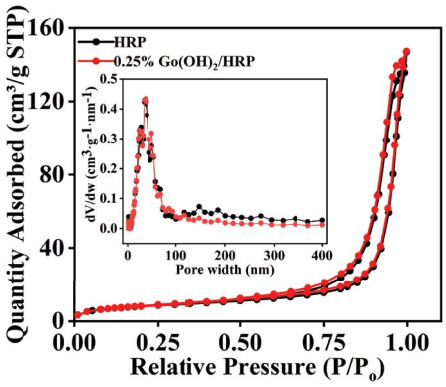

Fig. S2. Nitrogen adsorption–desorption isotherms and the corresponding pore size distribution curves (inset) of HRP and 0.25%$Co(OH)_2$/HRP.

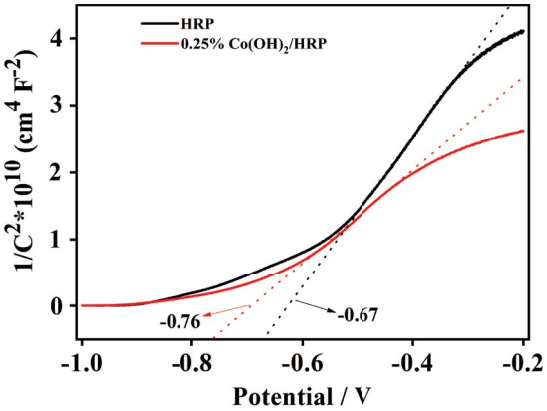

Fig. S4. Mott–Schottky plots of HRP and 0.25%$Co(OH)_2$/HRP composite.

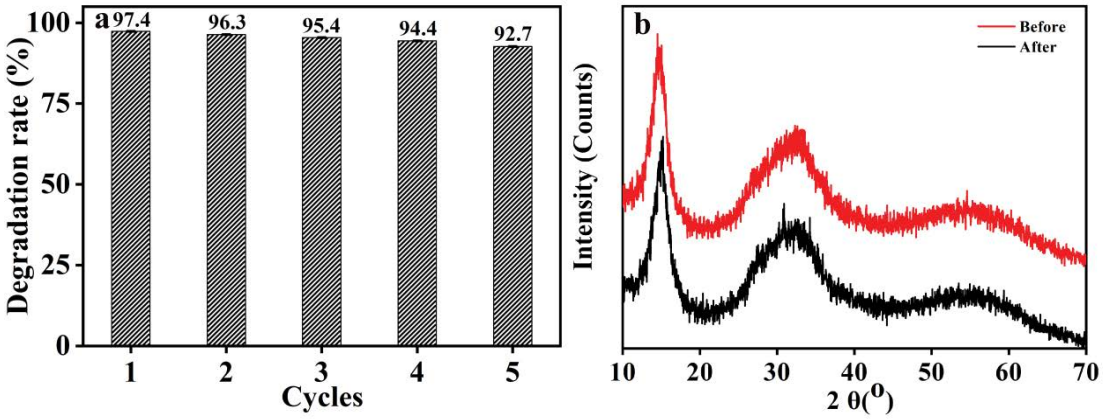

Fig. S3. (a) Curves of cyclic photodegradation of RhB by 0.25%$Co(OH)_2$/HRP and (b) XRD plots before and after cycling.